Nanoscale

PAPER

Cite this: *Nanoscale*, 2023, **15**, 1782

Electrochemically addressed FET-like nanofluidic channels with dynamic ion-transport regimes†

Gregorio Laucirica, [a] Yamili Toum Terrones, [a] Michael F. P. Wagner,[b] Vanina M. Cayón,[a] María Lorena Cortez, [a] Maria Eugenia Toimil-Molares,[b] Christina Trautmann,[b,c] Waldemar Marmisollé [a] and Omar Azzaroni *[a]

Received 17th August 2022,
Accepted 19th December 2022

DOI: 10.1039/d2nr04510a

rsc.li/nanoscale

Nanofluidic channels in which the ionic transport can be modulated by the application of an external voltage to the nanochannel walls have been described as nanofluidic field effect transistors (nFETs) because of their analogy with electrolyte-gated field effect transistors. The creation of nFETs is attracting increasing attention due to the possibility of controlling ion transport by using an external voltage as a non-invasive stimulus. In this work, we show that it is possible to extend the actuation range of nFETs by using the supporting electrolyte as a "chemical effector". For this aim, a gold-coated poly (ethylene terephthalate) (PET) membrane was modified with electroactive poly-*o*-aminophenol. By exploiting the interaction between the electroactive poly-*o*-aminophenol and the ions in the electrolyte solution, the magnitude and surface charge of the nanochannels were fine-tuned. In this way, by setting the electrolyte nature it has been possible to set different ion transport regimes, *i.e.*: cation-selective or anion-selective ion transport, whereas the rectification efficiency of the ionic transport was controlled by the gate voltage applied to the electroactive polymer layer. Remarkably, under both regimes, the platform displays a reversible and rapid response. We believe that this strategy to preset the actuation range of nFETs by using the supporting electrolyte as a chemical effector can be extended to other devices, thus offering new opportunities for the development of stimulus-responsive solid-state nanochannels.

Introduction

Throughout human history, nature has served as a model and mentor in a wide variety of fields including engineering, architecture, and art.[1–3] The concept "learning from nature" has been also extensively exploited in materials science and nanotechnology.[4] In particular, the outstanding properties of biological ion channels such as selectivity and rapid ion transport modulated by the environmental conditions have attracted the attention of the scientific community and have given rise to the development of fully-abiotic nanochannels with programmable ion transport known as solid-state nanochannels.[5,6] In comparison with biological channels and lipid membranes, solid-state nanochannels offer better mechanical and chemical stability which allows their use in a wide variety of environmental conditions that, even, might significantly differ from the biological environment.[7] However, the control of the ion transport properties is still below that of their biological counterparts. In this context, the development of fully-abiotic nanochannels with controlled ion transport properties and higher selectivity remains a great challenge.

The transport properties of solid-state nanochannels are typically regulated by the channel size and surface properties (*e.g.* charge and hydrophilicity).[6,8,9] Thus, changes in these parameters can promote changes in ion transport and, therefore, in the signal output (known as iontronic output). As an example, it is usually assumed that if the channel dimensions are comparable to the characteristic length of electrostatic interactions (Debye length: $\lambda_D \sim 3$ nm for 10 mM KCl), the magnitude of the surface charge density determines the ion concentration inside the channel and, concomitantly, the ion transport properties.[10,11] Therefore, chemical or physical

[a]*Instituto de Investigaciones Fisicoquímicas Teóricas y Aplicadas (INIFTA), Departamento de Química, Facultad de Ciencias Exactas, Universidad Nacional de La Plata, CONICET – CC 16 Suc. 4, 1900 La Plata, Argentina.*
E-mail: omarazzaroni@quimica.unlp.edu.ar
[b]*GSI Helmholtzzentrum für Schwerionenforschung GmbH, 64291 Darmstadt, Germany*
[c]*Technische Universität Darmstadt, Materialwissenschaft, 64287 Darmstadt, Germany*

†Electronic supplementary information (ESI) available: Additional material characterization by SEM, contact angle, and electrochemistry measurements. Also, it includes a scheme of the experimental setup and control experiments (iontronic output of PET/Au *vs.* V_g and iontronic output of POAP-modified membrane synthesized by using a different acid). See DOI: **https://doi.org/10.1039/d2nr04510a**

events that promote changes in the surface charge density can be used as ion transportation switches. Besides, asymmetries in the channel geometry cause a disruption in the electrical potential inside the channel implying the transport is characterized by a rectifying behavior, *i.e.* the ion current at one transmembrane voltage polarity is increased relative to the opposite polarity.[5,12–14] Due to the resemblance with diodes, this performance is often referred to as diode-like behavior. A distinctive feature of solid-state nanochannels with rectifying ion transport properties is that its iontronic output not only depends on the surface charge density but also on the polarity of the charges, *i.e.* the transmembrane voltage polarity where the current is enhanced (high conductance branch) is closely related to the type of the surface charges (positive or negative) whereas the efficiency of the rectification is related to the density of surface charges.[15–18]

In recent years, great efforts have been devoted to the development of stimuli-responsive nanodevices which enable the control of ion transport by applying different stimuli such as chemical effectors, pH, temperature, light, *etc.*[19–26] Particularly, the use of a non-invasive stimulus to switch ion transport properties is a desirable feature enabling new applications in fields such as filtration and controlled drug release.[27–29] As an example, the development of voltage-responsive nanodevices has been positioned as a great option due to the ability to control external voltages.[30–34] In this kind of device usually referred to as nanofluidic field-effect transistors (nFETs), the physicochemical characteristics of the nanochannel walls (hydrophobicity, electrostatic charge density) can be controlled by the application of an external voltage (so-called gate voltage $-V_g-$ in resemblance to the field-effect transistors –FETs–) generating different ion transport regimes. Typically, the creation of nFETs has involved subsequent depositions of semiconducting materials and gold layers.[33] However, in the last years, nFETs created by combining electroactive polymers (EPs) and nanofluidic devices have shown outstanding results characterized by their reversibility and rapid response.[30–32,35–37] EPs are formed by chains containing centers with the capability to reversibly alternate between different redox states.[38] EPs can be deposited as films on the nanochannels walls by physical,[19,30] chemical,[16,31] and electrochemical methods.[32,39] Usually, the change in the redox state of the EPs brings variations in the physicochemical properties of the polymer film (*e.g.* different charge states, volume, or wettability) that can be used to modulate the ion transport. By using this approach several devices can be created by combining different EPs and nanofluidic devices, however, the iontronic behavior is limited by the chemical nature of the oxidized and reduced states of the polymer.

Herein, the construction of a nanofluidic FET based on track-etched membranes containing single bullet-shaped nanochannels modified with the electroactive polymer poly-*o*-aminophenol (POAP) is reported. POAP is an electroactive polymer that presents two different redox states with their respective acid–base equilibria. Due to the differences in the protonation tendencies of both redox states, the charged state of the nanochannels surface at a given pH condition depends on the POAP redox state, which enables the control of the ion transport by the gating effect. Employing KCl as the supporting electrolyte, the rectification is varied from slightly positive rectifying to highly positive rectifying (anion-driven rectification) behavior by decreasing the V_g values. In this work, the actuation range could be extended by the adequate selection of the nature of supporting electrolytes. Employing K_2SO_4 as the supporting electrolyte, it is possible to further tune the rectification properties from highly negative rectifying (cation-driven rectification) to slightly negative rectifying behavior by switching the V_g values. Hence, this work introduces a new concept within bioinspired solid-state nanochannels based on EPs as it demonstrates that the selection of the actuation range is possible by choosing the adequate supporting electrolyte, and simultaneously, fine-tuning of the ion transport is achieved by controlling the external voltage.

Experimental section

Nanochannel fabrication

Ion transport experiments were performed with membranes that contain a single nanochannel created by ion-track-etching technology. For this, 12 μm polyethylene terephthalate (PET) membranes were irradiated with a single swift heavy ion (Au) with an energy of 5.9 MeV per nucleon. The irradiated membrane was subjected to UV light for 24 hours on only one side. After this, the membrane was immersed in a solution of 6 M NaOH + 0.05% w/w Dowfax 2a1 for 6 minutes at 60 °C.[40–42] The presence of surfactant in the etchant solution together with the UV light pretreatment enabled the creation of tapered channels with a bullet-shaped opening on one side denoted as channel tip. The channel openings on the other side of the foil are large and referred to as the base side. Prior to use, the membranes were immersed in milliQ® water for 4 hours. PET membranes irradiated with multiple ions (10^8 ions per cm^2) were used for geometrical characterization *via* scanning electron microscopy (SEM). In order to make possible the comparison of channels obtained in multi-pore membranes with those used in the ion transport experiments, UV light exposure and etching of both kinds of membranes were simultaneously performed. Finally, this procedure gives rise to bullet-shaped nanochannels with tip and base diameters around 107 ± 12 nm and 376 ± 30 nm, respectively (Fig. S1†).

Nanochannel modification

For the fabrication of the nFET, the PET membrane containing a single nanochannel was first coated with a thin layer (~100 nm) of gold on the tip side by sputtering (sputtering conditions: 30 mA, 0.1 mbar, and 100 s.) (Fig. 1a). Then, taking advantage of the electrical properties of the gold layer, a film of poly-*ortho*-aminophenol (POAP) was deposited *via* electropolymerization. For this, the Au-coated side of the membrane was exposed to a solution of 10 mM *ortho*-aminophenol (*o*-AP) in 0.1 M H_2SO_4 (unless otherwise specified) and the

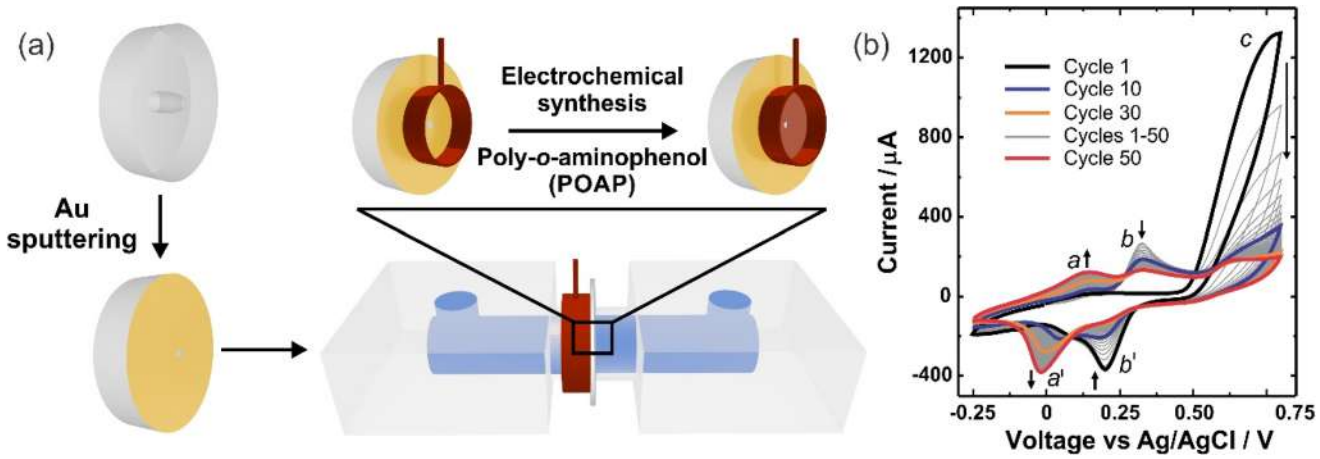

Fig. 1 (a) Scheme of nFET fabrication. PET membrane containing one single channel is sputter-coated with gold and then inserted into an electrolytic cell where is exposed to the *o*-AP solution. (b) *I*–*V* curve for the electropolymerization of 10 mM *o*-AP in 0.1 M H_2SO_4.

bias voltage was swept from −0.25 to 0.8 V for 50 cycles at 100 mV s^{-1} using a Pt coil and Ag/AgCl (3 M NaCl) as counter and reference electrodes, respectively (the gold side of the membrane acted as working electrode working area = 0.463 cm^2) (Fig. 1a).[43–45] Voltage control and current measurement were performed using a potentiostat Gamry Reference 600+.

Membrane characterization

In addition to electrochemical measurements, the modified membrane was characterized by Raman spectroscopy, Scanning Electron Microscopy – Energy Dispersive X-ray spectroscopy (SEM-EDX), and contact angle measurements. Raman spectroscopy was performed with a Raman Fiber Probes from HORIBA Scientific with a green fiber optic laser 532 nm, SEM-EDX analyses were done by using a Zeiss Gemini 500 and, finally, contact angle images were obtained with an optical tensiometer Theta Lite by Biolin Scientific. Detailed analysis of the membranes at each modification step by EDX and contact angle is presented in the ESI file.†

Gate-controlled measurements

Conventional electrochemical experiments (*i.e.* electropolymerization, gate control, and electrochemical measurements) were performed using a three-electrode arrangement connected to a potentiostat Gamry Reference 600+. In all cases, the Au-coated side of the membrane acted as the working electrode whereas a Pt coil and Ag/AgCl (3 M NaCl) were the counter and reference electrodes, respectively. Ion transport experiments (iontronic measurements) were obtained by using a two-electrode (both Ag/AgCl/3 M NaCl) arrangement connected to a potentiostat Gamry Reference 600. In the case of ion transport experiments with controlled gate voltage (V_g), the curves were recorded by working with the aforementioned systems coupled (bipotentiostat mode) (see further details in the ESI file†). The different experiments were performed using solutions 0.1 M of K_2SO_4 and KCl at pH 2 (unless otherwise stated).

Rectification factor (f_{rec})

In order to quantify the rectification efficiency, the rectification factor (f_{rec}) is defined as follows,

$$f_{rec} = \left|\frac{I(+1\,V)}{I(-1\,V)}\right| \text{ if } I(+1\,V) > |I(-1\,V)|$$

or,

$$f_{rec} = -\left|\frac{I(-1\,V)}{I(+1\,V)}\right| \text{ if } |I(-1\,V)| > I(+1\,V)$$

Considering that the current in the numerator is that of the high conductance branch, $|f_{rec}| > 1$. If the high conductance branch is placed at positive transmembrane voltages, f_{rec} takes positive values (>1). On the contrary, if the high conductance branch is placed at negative transmembrane voltages, f_{rec} takes negative values (<−1). Therefore, by using this definition, the magnitude of the surface charge density is related to $|f_{rec}|$ whereas the sign of f_{rec} indicates the polarity of the surface charge.[15]

Results and discussion

Fig. 1b shows the voltammograms corresponding to the POAP electrosynthesis. The first positive cycle of electropolymerization of *o*-AP is characterized by a high increase in the current at bias voltage values around 0.6 V–0.8 V due to the oxidation of *o*-AP to form the monocation radical (peak c) (without its complementary reduction peak).[46,47] After the first scan, the voltammograms evidence two additional quasi-reversible redox couples (pairs a–a′ and b–b′) with medium peak potentials $-E_{1/2}-$ (defined as the potential average of the oxidation and reduction peaks) at 0.05 V and 0.25 V, respectively. The redox pair placed at 0.05 V displays a continuous increase of the current as the number of cycles is increased which is a distinctive behavior of electrodeposited electroactive substances, and therefore, it evidences the formation of the POAP film

onto the Au-coated side of the membrane (PET/Au/POAP).[48] For its part, the peak pair at 0.25 V exhibits a decrease in the current as the number of cycles increases which is ascribed to the formation of soluble products. Details about the reaction mechanism have been previously reported.[43,46]

Each modification step was studied by material characterization (SEM/EDX, Raman spectroscopy, and contact angle) and electrochemical techniques. Fig. 2a shows the SEM micrographs for a multi-pore PET membrane (10^8 pores per cm^2) created by the UV-assisted etching.[40] From the SEM image analysis, average values of the tip and base diameters of 110 ± 10 nm and 380 ± 30 nm, respectively, could be determined (Fig. 2a(i) and Fig. S1†). The channels have a cylindrical shape along most of the cross-section and in the final hundreds of nanometers, a tapered with a parabolic profile characteristic of the bullet-shaped geometry (Fig. 2a(ii)).

Although there were several previous works related to the construction of Au-coated membranes for the development of nFET, some aspects of gold deposition remained unclear. After gold sputtering onto the tip side to form PET/Au, SEM images revealed a partial diminution in the tip diameter to values around 70 ± 10 nm (Fig. 2b(i)). This trend has been reported in previous works related to the development of nFETs.[32,35] Interestingly, the cross-section image of the PET/Au membrane evidenced the presence of a gold layer with a thickness of around 100 nm on the external side of the membrane (Fig. 2b (ii)). Only little amounts of gold are found in the first few nanometers inside the channel suggesting a very low penetration range of the metal and therefore, the formation of an asymmetric device not only in its geometry but also from a chemical point of view. EDX analysis confirms the presence of gold only on the tip side of the PET membrane (Fig. S2a†). On this side, the contact angle displayed a value of ~80° due to the hydrophobicity of gold compared to 68° of PET (Fig. S2b†).[16]

After electropolymerization, the tip diameter was further reduced to around 45 ± 6 nm which evidences a partial reduction in the tip diameter due to the POAP film integration (Fig. 2c(i)).[32,35,49] The presence of a thin compact film of POAP was also evidenced in the top-view SEM images as a change in the contrast regarding the non-modified region. Also, considering the colored nature of this polymer, the film deposition results in the appearance of the characteristic brown color on the gold layer (Fig. S2d†). The contact angle displayed an appreciable diminution in the value from 80° (gold surface) to

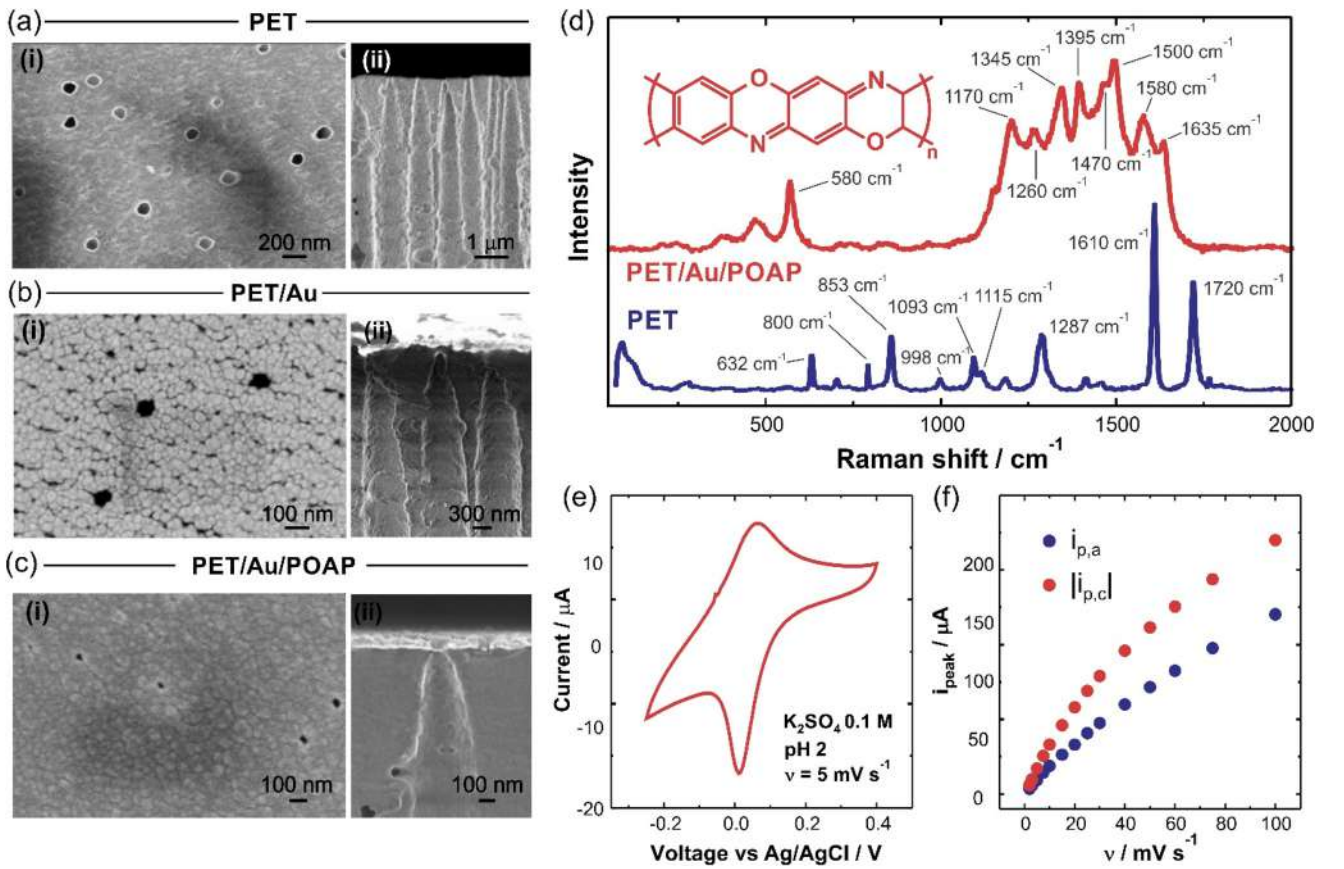

Fig. 2 SEM images of the (i) tip side and the (ii) cross-section of the different modification steps of the PET membranes. (a) PET membrane containing bullet-shaped nanochannels. (b) Gold-coated PET membrane containing bullet-shaped nanochannels (PET/Au). (c) The final POAP-modified membrane (PET/Au/POAP). (d) Raman spectra obtained of the surface of PET (blue) and PET/Au/POAP (red) multipore membranes. (e) Electrochemical response of POAP-modified membrane in 0.1 M K_2SO_4 pH = 2 at a scan rate ν = 5 mV s^{-1}. (f) Current densities (j) for the anodic ($j_{p,a}$) and cathodic ($j_{p,a}$) peaks at different scan rates. Electrochemical measurements were performed with a working area = 0.463 cm^2.

56° due to the higher hydrophilicity of this electroactive polymer (Fig. S2c†). The POAP film thickness was estimated through the cathodic charge as ~23 nm and, considering that the gold layer is only a few nanometers inside of the channel, it is expected that the POAP film is only on the external surface and in the entrance region of the channel (Fig. 2c(ii)).[50]

The POAP film integrated onto the Au-coated membrane was characterized by Raman spectroscopy, X-ray photoelectronic spectroscopy (XPS) and electrochemical measurements (Fig. S3 and S4†). Fig. 2d shows the Raman spectrum obtained from the POAP surface. The spectrum not only presents the typical characteristic peaks obtained for electroactive polymers based on substituted anilines but also is in excellent agreement with previously reported spectra for POAP.[51,52] XPS spectra and a detailed assignment of Raman peaks are presented in the ESI file.†

The cyclic voltammetry (CV) showed the presence of only one redox pair (Fig. 2e). The position and shape of the peaks are in strong agreement with previous works, *i.e.* the voltammetry curve of POAP is characterized by a broad oxidation peak and a slimmer reduction peak with an $E_{1/2}$ around ~50 mV *vs.* Ag/AgCl.[35] The difference between the potentials for the cathodic (*i.e.* reduction reaction; $E_{p,c}$) and anodic (*i.e.* oxidation reaction; $E_{p,a}$) peaks is smaller than 59 mV which is a characteristic behavior in the reaction of redox couples onto surfaces.[48,53] Also, the study of the redox performance at different scan rates evidenced the typical behavior reported for POAP-modified electrodes characterized by a linear relationship between the peak current and scan rate (ν) for small ν values (<10 mV s^{-1}) (Fig. 2f).[35] Further analysis of POAP electrochemical response for both supporting electrolytes is available in the ESI file.†

Furthermore, the success of each modification step was evidenced *via* the measurement of ion transport across the membrane using different electrolytes. Initially, the ion transport across the PET membrane displayed an ohmic behavior in K_2SO_4 and KCl solutions at pH 2 which is attributed to the null surface charge. This fact is explained by the predominance of protonated carboxylic acids ($pK_a \sim 3.7$) over the carboxylate groups on the nanochannel walls due to the highly acidic pH condition (Fig. 3a). Also, the different slopes in the *I–V* curves arise from the differences in the inherent conductance of each salt. In particular, the increment in the ion current due to the replacement of chloride ions with sulfate anions has been comprehensively studied in ref. 54. After the deposition of the gold layer onto the tip side of the membrane (PET/Au), the nanofluidic device exhibited a rectifying behavior characterized by an increase in the currents at negative transmembrane voltages (Fig. 3b). This kind of rectifying transport is typically seen in geometrically asymmetric channels with negatively charged walls (so-called cation-selective or cation-driven rectification) and, in this case, these negative charges are ascribed to the anion adsorption onto the gold surface.[55,56] The subsequent POAP deposition onto the gold surface (PET/Au/POAP) triggered changes in the iontronic output with evident variations depending on the anion nature (Fig. 3c). Thus, the response for KCl exhibited a low rectification behavior characterized by an increase in the currents at positive transmembrane voltages which is proper for asymmetrical channels with positively charged walls (so-called anion-selective rectification or anion-driven rectification) (Fig. 3c –red curve–). This fact was previously reported and can be attributed to the presence of positively charged amino/imino groups from POAP film at open circuit potential conditions (~0.1 V), *i.e.* when no voltage is applied to the POAP layer.[35] In contrast, when the supporting electrolyte is K_2SO_4, the response evidenced a cation-driven rectification which is indicative of a predominance of negative charges onto the channel surface (Fig. 3c –blue curve–). The inversion in the surface charge for the case of K_2SO_4 supporting electrolyte with respect to the KCl case could be explained due to local inversion of charge promoted by the interaction between SO_4^{2-} with both positively charged amino centers from POAP and the gold surface. On the one hand, the charge inversion or attenuation assisted by the interaction between amino groups and multivalent anions (*e.g.* PO_4^{3-} and SO_4^{2-}) has been extensively studied in previous reports for different systems ranging from nanochannels, flat surfaces, and colloidal particles.[15,57–61] The entrance of ions to the POAP polymer film from supporting electrolytes has been previously reported by electrochemical quartz crystal microbalance experiments.[62] XPS experiments confirm the presence of sulfate and chloride ions associated with POAP films after cycling into K_2SO_2 and KCl pH 2 solutions, respectively (for a detailed description, see ESI file Fig. S3†). Furthermore, compared to the results obtained in KCl, the zeta potential of a POAP dispersion displayed an attenuation in its magnitude when was evaluated in K_2SO_4 at pH = 2 due to the interaction between HSO_4^- and SO_4^{2-} and amino/imino groups from POAP (see Fig. S5†). The diminution of the surface charge caused by the interaction with sulfate anions has been also explored using a negatively charge redox probe on the POAP electrode (Fig. S11†). Analogously, similar behaviors are obtained for the case of carboxylate groups with cations such as Ca^{2+}.[63] On the other hand, resistometric measurements of POAP-modified electrodes have evidenced the adsorption of HSO_4^- and SO_4^{2-} on the gold surface.[64] Consequently, the cooperative effect of these two phenomena added to the multivalent nature of SO_4^{2-} makes the inversion in the overall surface charge possible regarding the behavior observed for KCl.

Dependence on gate voltage V_g

Considering the electroactive nature of POAP, the modulation of an external voltage allows controlling the redox state of the polymer. Consequently, the differences in the chemical nature between the oxidized and reduced states of the electroactive polymer might trigger variations in the transport properties of the single nanochannel and concomitantly, in the iontronic signal. Thus, in analogy to electrolyte-gated FETs where the application of an external voltage (referred to as gate voltage, V_g) enables modulating the electronic current flowing between the drain and source electrodes (at a given voltage between

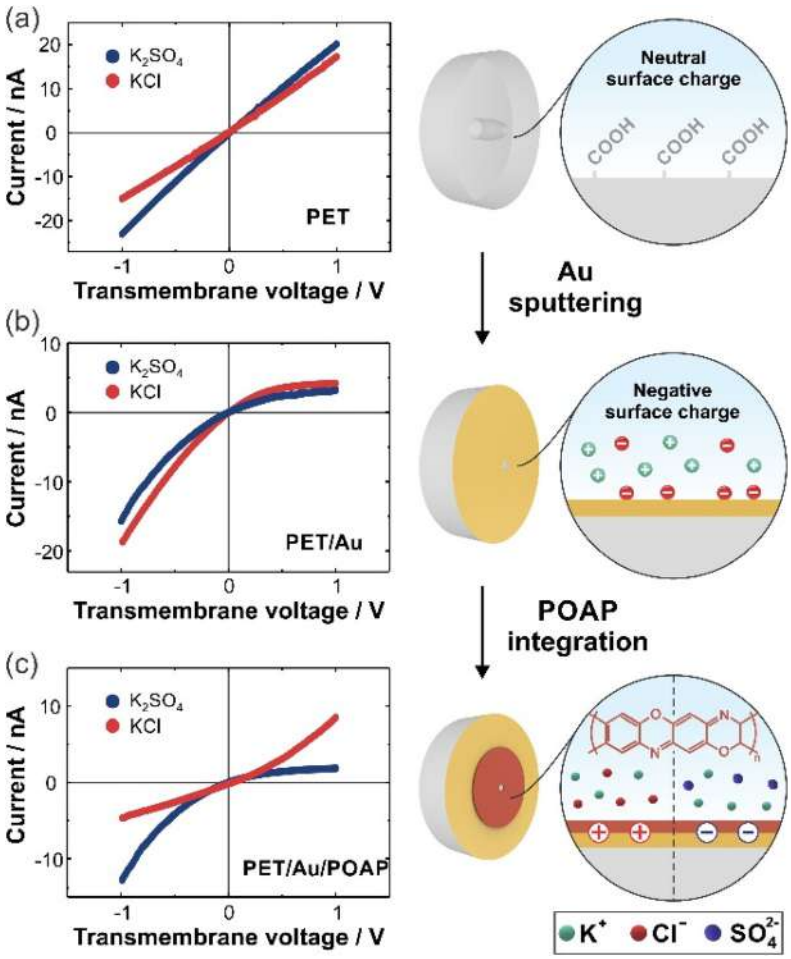

Fig. 3 Scheme of the different modification steps and their respective experimental iontronic responses: (a) PET, (b) PET/Au and (c) PET/Au/POAP. The dotted line in scheme (c) indicates the effects on the surface when PET/Au/POAP is exposed to K_2SO_4 (right) and KCl (left). All the experiments were performed at pH = 2 and analytical concentration of 0.1 M.

drain and source, V_{DS}), it is expected that the control of an external voltage enables to modulate the ion current magnitude across the PET/Au/POAP membrane (Scheme 1). To study the performance of PET/Au/POAP membrane as a FET-like nanofluidic device (or nFET),[35] *I–V* curves were recorded by applying different external voltages to the POAP layer (see the ESI file for further details on the experimental set-up Fig. S6†). Due to the resemblance of this kind of device with FETs, the external voltage will be referred to as gate voltage –V_g–.

Fig. 4 shows the *I–V* curves obtained for different V_g in the presence of K_2SO_4 and KCl at pH = 2. When the supporting electrolyte is KCl, the rectifying behavior is characterized by an increment in the current at positive transmembrane voltages which, as explained above, evidences the presence of positively charged sites on the channel walls (Fig. 4a). Changing V_g from 0.2 V to −0.2 V makes POAP going from an oxidized state to a reduced state (Fig. 2e). As spectroelectrochemical studies have demonstrated, the protonation tendency of amine groups in the reduced state of POAP exceeds the protonation tendency of imine groups in its oxidized state, and therefore, it is clear that, at pH 2, the reduced state at V_g = −0.2 V will be the higher charged state of the polymer.[45,62] In line with these assumptions, the *I–V* curves (Fig. 4a) show how the transmembrane currents at positive potentials grow when going from V_g = 0.2 V (oxidized state) to V_g = −0.2 V (reduced state). As a consequence of such increases in the charged state promoted by the POAP reduction, the analysis of the rectification factor in terms of V_g shows an increment in the rectification factor f_{rec} as V_g decreases from 0.2 V to −0.2 V (Fig. 4c –red points–). Furthermore, the range of V_g where the ion transport could be modulated by the external voltage was found to be in good agreement with the position of the redox peaks in the voltammogram of POAP presented in Fig. 2e which supports the hypothesis that the chemical redox transformation is responsible for the stimulus-responsive actuation. To illustrate this point, the voltammetric charge of the reduction peak at the different V_g was included in Fig. 4c (gray empty circles). The value arising from the integration of the peak for different voltages represents a measure of the reduced (or oxidized) amount of EP at a given voltage.[48] Considering the kinetic

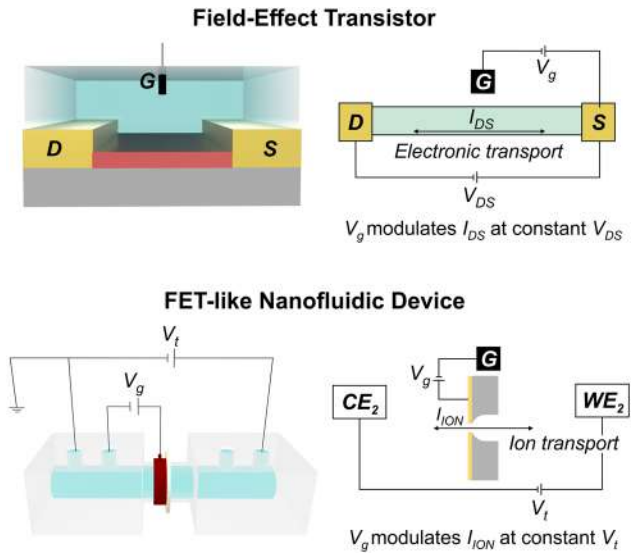

Scheme 1 Schematic illustration of the analogy between electrolyte-gated Field-Effect Transistors (FETs) and FET-like nanofluidic devices (or nFET). The magnitude of V_g allows modulating the extent of electronic current (I_{DS}) flowing between the drain (D) and source (S) electrodes. V_{DS} represents the voltage between D and S. In the nFET, the external voltage modulates the magnitude of the ion current (I_{ION}) at a given transmembrane voltage (V_t). In this case, V_g is directly applied to the Au-layer on the tip side of the membrane whereas the transmembrane voltage is controlled by employing an independent two-electrode set-up consisting of two Ag/AgCl electrodes.

implications of the cyclic voltammetry technique, the voltammetric charge calculation was carried out by subtracting the capacitive component of the current in the cyclic voltammetry recorded in 0.1 M K_2SO_4 pH 2 at a low scan rate (5 mV s^{-1}). Then, the voltammetric integrated charge in Fig. 4c (gray empty points) behaves as the reduction degree of the POAP film at each voltage. Similarities of the sigmoidal response among rectification factors in each electrolyte and the reduction degree as a function of the gate voltage confirm the coupling of the iontronic response with the redox state of the polymer film.

On the contrary, when the supporting electrolyte is composed only of K_2SO_4, the *I–V* curve presents a cation-driven rectification regime (Fig. 4b). When V_g is diminished from 0.2 V to −0.2 V, an evident diminution (increment) in the current modules at negative (positive) transmembrane voltage is produced. Thus, the rectification factor displayed a decrease (in module) as V_g was decreased from 0.2 V to −0.2 V. The behavior displayed in the presence of K_2SO_4 seems to indicate the presence of sulfate anions bound on the POAP and gold film generating a predominance of negative charges on the surface. The decrease of $|f_{rec}|$ due to the switching of V_g from 0.2 V to −0.2 V can be explained due to the POAP reduction and, therefore, the generation of protonated amino groups (positively charged sites) that partially neutralizes the negatively charged sites. Similar, to the KCl case, there is a good correlation between the region of changes in f_{rec} and the voltage window where the POAP film is reduced.

It is worth mentioning that control experiments performed in PET/Au with both electrolytes did not show significant changes in the ion transport properties by varying V_g which allows asserting that the voltage-responsiveness of PET/Au/POAP in both cases is explained by the presence of the POAP film rather than the changes in the gold surface charge due to the polarization (Fig. S7†).[35] Furthermore, there are almost no changes in the contact angle either due to the nature of the supporting electrolyte or the change in the redox state of the POAP[35] which seems to indicate that the modulation in the ion transport is mainly controlled by the changes in the surface charge (Fig. S2†). Moreover, the iontronic output observed for the different salts was found independent of the acid used during the electropolymerization of POAP, *i.e.* the behavior in presence of the different salt natures was qualitatively the same for POAP films synthesized in both H_2SO_4 and $HClO_4$ media, and, also, the trends were reproducible in independent samples (Fig. S8 and S9†).

In view of the presented results, the integration of a POAP film onto the Au-coated PET membrane allows the modulation of ion transport by tuning the external voltage (gate voltage) and the choice of the electrolyte. This fact stems from the

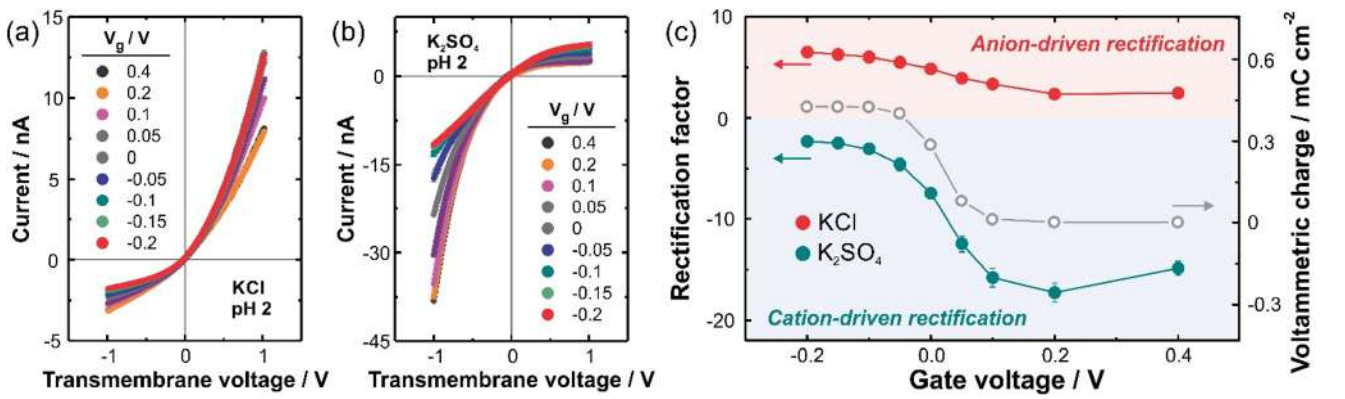

Fig. 4 *I–V* curves at different gate voltages in presence of 0.1 M (a) KCl and (b) K_2SO_4 (pH = 2). (c) Variation in the rectification factor in terms of gate voltage for the different electrolytes. Also, the changes in the voltammetric charge at the different external voltages are shown (gray points).

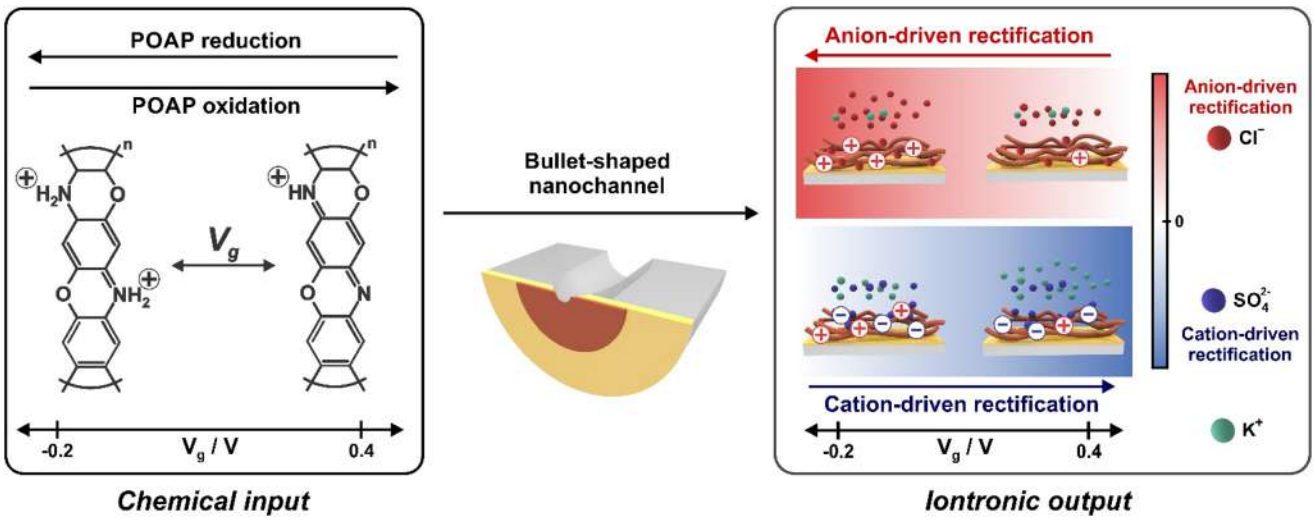

Scheme 2 Scheme illustrating the relationship between the chemical input and the concomitant iontronic output proposed for the nanodevice PET/Au/POAP at pH 2. The interplay between the redox transformation of POAP and its interaction with counterions available in the supporting electrolyte gives rise to a fine-tune modulation of rectification properties among cation-driven rectification, non-rectifying, and anion-driven rectification.

changes in the charged state of POAP during the redox reaction (chemical input). Thus, in presence of potassium chloride, the response can be modulated from low-selective behavior (low rectification) to anion-selective behavior (high anion-driven rectification) by varying the gate voltage from 0.4 V to −0.2 V (Scheme 2 (red blocks)) which arises from the higher protonation tendency of the reduced POAP in comparison with the oxidized state. Instead, in presence of potassium sulfate, the response can be modulated from cation-selective behavior (high cation-driven rectification) to a low-selective behavior (low rectification) by varying the gate voltage from 0.4 V to −0.2 V due to the coexistence of two different phenomena. On the one hand, the sulfate ions adsorbed on the POAP film and gold surface generate a global negative charged film (Scheme 2 (blue blocks)). On the other hand, the reduction of POAP film due to the diminution of V_g promotes the increment in the charge of the POAP film. The trade-off between these phenomena results in the diminution of the global negative charge as the V_g is diminished (V_g switched from oxidation values to reduction values). Interestingly, these results show the capability to modulate the dynamic range of actuation in nFETs based on electroactive polymers with acid–base groups by the appropriate selection of the supporting electrolyte (salt nature). While local charge reversion due to the presence of multivalent anions has been previously reported in different systems, usually those works use the nature of the anion (or cation) as the stimulus and thus, the extent (and direction) of the rectification is varied by setting the anion concentration.[15,59,65–67] In the present work, the stimulus is the external voltage (V_g) and at the same time, the nature of the salt determines the rectifying regime of the diode.[68] Consequently, the interplay between V_g (non-invasive stimulus) and the identity of the supporting electrolyte makes possible the fine-tune modulation of the rectifying properties among different states such as cation-driven, anion-driven, and non-rectifying regimes, in order to create versatile solid-state nanochannels-based devices.

pH influence

To gain insight into this peculiar behavior, the response of the device was studied at different pH values employing both KCl and K_2SO_4 as supporting electrolytes (Fig. 5). Interestingly, in both cases, the increment in the pH value of the supporting electrolyte promotes profound changes in the rectification factor values. However, as the dynamic range of the device in each case is different, the changes in the iontronic output are highly dependent on the salt nature. In the case of KCl, the rectification was turned off as the pH increased (f_{rec} from positive values to ~1) (Fig. 5a–c). This behavior is ascribed to the deprotonation of imino and amino-charged groups of POAP and therefore, the loss of the positively charged sites into the film for both reduced and oxidized states.

In contrast, as in presence of sulfate salt the device acts as a cation-selective nanochannel (negative rectification factors), the loss of positively charged sites in the POAP film leads to more negative rectification factors (increase in the module), and therefore, as the pH increase, the device shows a more efficient rectifying regime (higher $|f_{rec}|$ values) (Fig. 5c–e). It is worth mentioning that sulfate has also its acid–base equilibrium (pK_a (HSO_4^-) ~ 2). In particular, when the pH rises, the ratio of SO_4^{2-}/HSO_4^- increases, which contributes, in addition to the POAP charge loss, to the increment in the negative surface charge and, concomitantly, in the rectification module.

On the other hand, for both supporting electrolytes, the increment of the pH value leads to a partial loss of the revers-

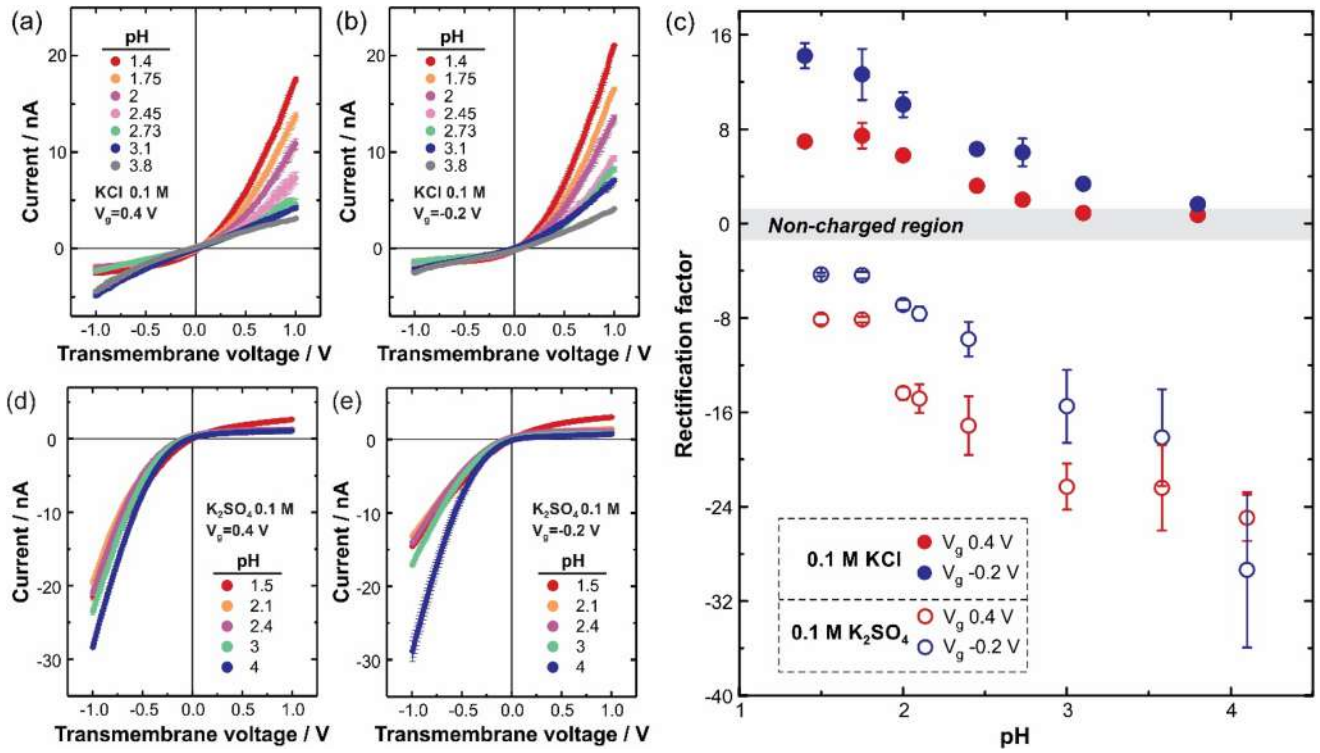

Fig. 5 *I–V* curves at different pH values at (a) V_g = 0.4 V (b) V_g = −0.2 V in 0.1 M KCl. (c) Variation in the rectification factor at 0.4 V and −0.2 V as the pH is increased for KCl. *I–V* curves at different pH values at (d) V_g = 0.4 V (e) V_g = −0.2 V in 0.1 M K_2SO_4. (c) Variation in the rectification factor at 0.4 V and −0.2 V as the pH is increased for K_2SO_4.

ible electrochemical transformation for the POAP film which contributes to hide the voltage-driven switchability of the ion transport in PET/Au/POAP (see ESI file for further details on the dependence between POAP electrochemical performance and pH Fig. S10†). This trend is typically observed in most of the electroactive polymers based on substituted anilines and it is the reason why the experiments are mostly performed at pH = 2.[32,35]

Last but not least, the reversible and rapid response of the device against a given stimulus is highly desirable in stimulus-responsive nanodevices with tailorable ion transport properties. In this particular case, as the supporting electrolyte acquires a central role not only in the ion transport but also influencing the redox processes in the stimulus-responsive building block (POAP), the switchability and kinetic of the response become crucial. Thus, both the nanodevice switch-

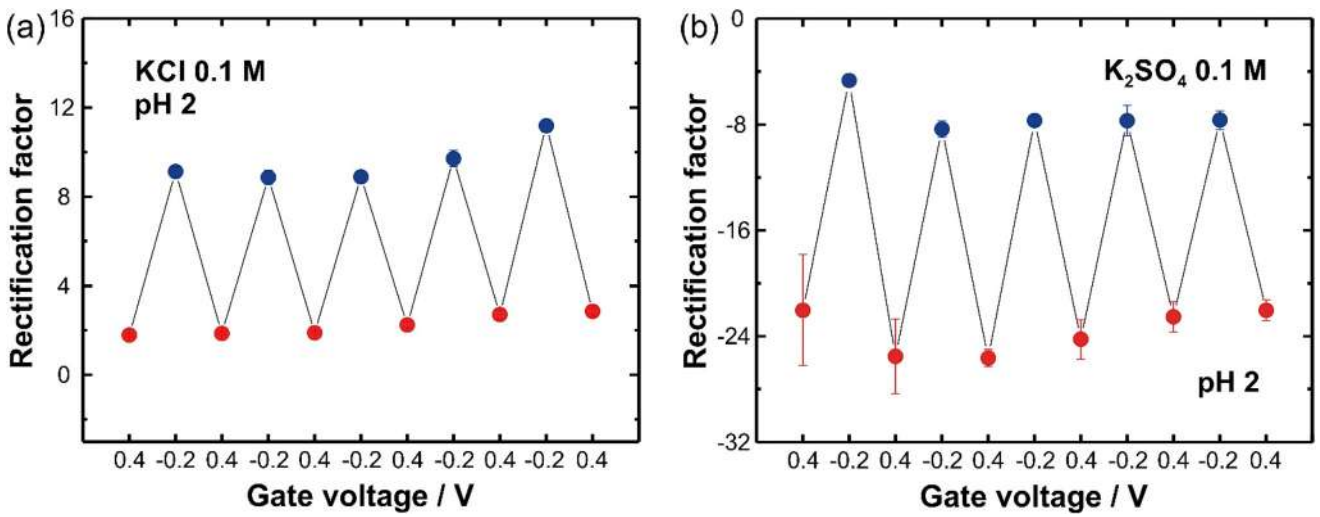

Fig. 6 Reversibility test in presence of 0.1 M (a) KCl and (b) K_2SO_4 at V_g = 0.4 and −0.2 V (pH = 2).

ability and transition kinetics between 0.4 V and −0.2 V were tested using the different salts as supporting electrolytes (Fig. 6 and 7). For instance, in presence of KCl, the device alternated from lower rectifications to higher rectifications by switching the V_g between 0.4 V and −0.2 V, respectively (Fig. 6a). The reason for this behavior also stems from the possibility to increase the charged state of POAP *via* its reduction reaction. In the case of K_2SO_4, the response could be alternated from higher rectifications to lower rectifications (in module) by switching the V_g between 0.4 V and −0.2 V (Fig. 6b). Therefore, in both supporting electrolytes, the response exhibited good reversibility for at least five cycles.

The kinetic study was performed by measuring the transient current when V_g was switched from 0.4 V to −0.2 V. In the case of KCl, the ion current was recorded at V_t = 1 V whereas, in the case of K_2SO_4, the ion current was recorded at V_t = −1 V. The choice of the transmembrane voltage is due to the more pronounced differences in the ion currents at those transmembrane voltages in PET/Au/POAP. When the experiment was performed with KCl, the ion current at +1 V showed an abrupt increment when the V_g varied from 0.4 V to −0.2 V (Fig. 7a). In contrast, the ion current at V_t −1 V abruptly decreased (in module) for the same stimulus in presence of K_2SO_4 (Fig. 7b).

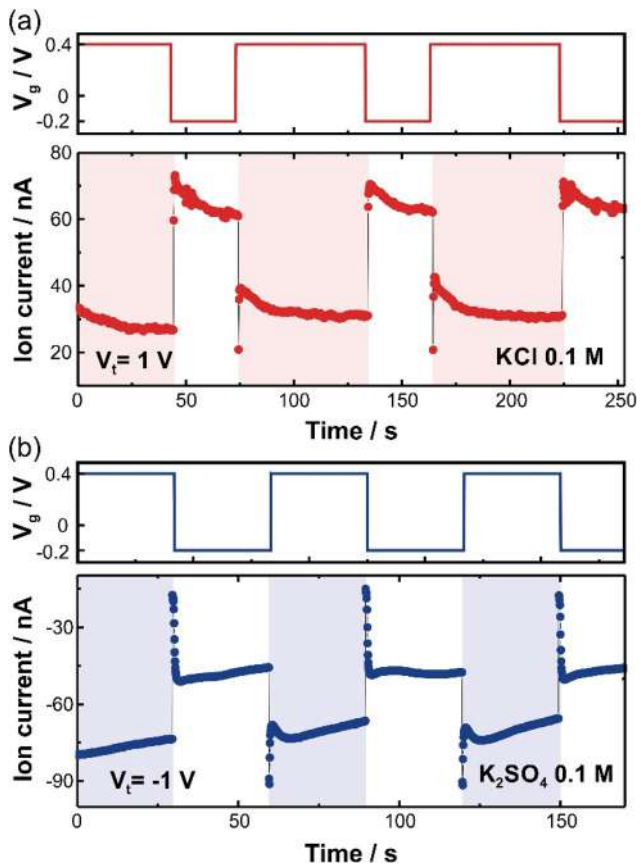

Fig. 7 Kinetic study of the transient current when switching V_g between two values (0.4 V and −0.2 V) for 0.1 M (a) KCl and (b) K_2SO_4 at pH = 2.

In both cases, the results agree with the trend observed in the *I–V* curves at different V_g (Fig. 4). Furthermore, in the presence of both salts, the PET/Au/POAP displayed a rapid and reproducible response against the gate voltage. As reported earlier by Pérez-Mitta *et al.*, the iontronic signal shows a trend closely related to the electrochemical response of the polymer.[31] Concomitantly, the ion transport could be rapidly established in the different redox states of POAP which is a very interesting property from a technological perspective.

Conclusions

In summary, we clearly showed that modifying track-etched membranes with a gold layer and then, an electroactive polymer (POAP) film provides an extended range of actuation. The integration of POAP is simply achieved by electropolymerization of the monomer 2-aminophenol. The geometrical asymmetry of the channel together with the presence of an electroactive polymer film on the outer surface and the tip region makes it possible to easily tune the ion transport properties of the channel by manipulating the external voltage. Interestingly, in addition to previous works related only to external voltage-controlled nanodevices, the capability to set the actuation range by selecting the nature of the electrolyte is demonstrated. More in detail, the possibility to modulate the ion transport among three rectification regimes (non-selective, cation-driven, and anion-driven) is achieved by taking advantage of the interplay between the positively charged sites of the polymer and their interaction with the counter-ions present in the solution. Controlling the polymer redox state by applying different external voltages also allows fine-tuning of the rectification efficiency. Furthermore, the ion transport at different external voltages and in presence of different supporting electrolytes displayed both a rapid response as well as reversible properties for at least five cycles. We believe that this strategy that combines responsiveness to non-invasive external stimuli and actuation range modulation by the appropriate selection of supporting electrolytes paves the way to a wide range of new solid-state nanochannel-based platforms with promising applications in matter manipulation in integrated circuits.

Conflicts of interest

There are no conflicts to declare.

Acknowledgements

G. L. and Y. T. T. acknowledge the scholarship from CONICET. G. L. also acknowledges a scholarship for a research stay from German Academic Exchange Service (DAAD) and the support of the GET_INvolved program of the GSI, Darmstadt (Germany). V. M. C. acknowledges the postdoctoral financial support from Universidad Nacional de La Plata. M. L. C., W. A. M., and O. A. acknowledge the financial support from

Universidad Nacional de La Plata (PPID-X867), CONICET (PIP-0370), and ANPCyT (PICT-2017-1523 and PICT2016-1680). The irradiated PET foils are part of the experiment UMAT, which was performed at the beam line X0 at the GSI Helmhotzzentrum für Schwerionenforschung, Darmstadt (Germany) in the frame of FAIR Phase-0.

References

1 R. L. Ripley and B. Bhushan, *Philos. Trans. R. Soc., A*, 2016, **374**, 20160192.
2 Y. H. Cohen and Y. Reich, *Biomimetic Design Method for Innovation and Sustainability*, Springer International Publishing, Cham, 1st edn, 2016.
3 A. Gleich, C. Pade, U. Petschow and E. Pissarskoi, *Potentials and Trends in Biomimetics*, Springer Berlin Heidelberg, Berlin, Heidelberg, 1st edn, 2010.
4 B. Bhushan, *Philos. Trans. R. Soc., A*, 2009, **367**, 1445–1486.
5 Z. Zhang, L. Wen and L. Jiang, *Chem. Soc. Rev.*, 2018, **47**, 322–356.
6 G. Pérez-Mitta, A. G. Albesa, C. Trautmann, M. E. Toimil-Molares and O. Azzaroni, *Chem. Sci.*, 2017, **8**, 890–913.
7 S. Howorka and Z. Siwy, *Chem. Soc. Rev.*, 2009, **38**, 2360–2384.
8 G. Pérez-Mitta, M. E. Toimil-Molares, C. Trautmann, W. A. Marmisollé and O. Azzaroni, *Adv. Mater.*, 2019, **31**, 1901483.
9 Q. Ma, Z. Si, Y. Li, D. Wang, X. Wu, P. Gao and F. Xia, *TrAC, Trends Anal. Chem.*, 2019, **115**, 174–186.
10 R. B. Schoch and P. Renaud, *Appl. Phys. Lett.*, 2005, **86**, 253111.
11 R. B. Schoch, J. Han and P. Renaud, *Rev. Mod. Phys.*, 2008, **80**, 839–883.
12 Z. S. Siwy, *Adv. Funct. Mater.*, 2006, **16**, 735–746.
13 X. Hou, H. Zhang and L. Jiang, *Angew. Chem., Int. Ed.*, 2012, **51**, 5296–5307.
14 G. Laucirica, A. G. Albesa, M. E. Toimil-Molares, C. Trautmann, W. A. Marmisollé and O. Azzaroni, *Nano Energy*, 2020, **71**, 104612.
15 G. Laucirica, G. Pérez-Mitta, M. E. Toimil-Molares, C. Trautmann, W. A. Marmisollé and O. Azzaroni, *J. Phys. Chem. C*, 2019, **123**, 28997–29007.
16 G. Laucirica, M. E. Toimil-Molares, C. Trautmann, W. A. Marmisollé and O. Azzaroni, *ACS Appl. Mater. Interfaces*, 2020, **12**, 28148–28157.
17 I. Vlassiouk and Z. S. Siwy, *Nano Lett.*, 2007, **7**, 552–556.
18 G. Pérez-Mitta, A. Albesa, F. M. Gilles, M. E. Toimil-Molares, C. Trautmann and O. Azzaroni, *J. Phys. Chem. C*, 2017, **121**, 9070–9076.
19 G. Laucirica, Y. Toum Terrones, V. M. Cayón, M. L. Cortez, M. E. Toimil-Molares, C. Trautmann, W. A. Marmisollé and O. Azzaroni, *Nanoscale*, 2020, **12**, 18390–18399.
20 V. M. Cayón, G. Laucirica, Y. Toum Terrones, M. L. Cortez, G. Pérez-Mitta, J. Shen, C. Hess, M. E. Toimil-Molares, C. Trautmann, W. A. Marmisollé and O. Azzaroni, *Nanoscale*, 2021, **13**, 11232–11241.
21 G. Pérez-Mitta, J. S. Tuninetti, W. Knoll, C. Trautmann, M. E. Toimil-Molares and O. Azzaroni, *J. Am. Chem. Soc.*, 2015, **137**, 6011–6017.
22 M. Liu, H. Zhang, K. Li, L. Heng, S. Wang, Y. Tian and L. Jiang, *Adv. Funct. Mater.*, 2015, **25**, 421–426.
23 H. Zhang, X. Hou, J. Hou, L. Zeng, Y. Tian, L. Li and L. Jiang, *Adv. Funct. Mater.*, 2015, **25**, 1102–1110.
24 Y.-B. Zheng, S. Zhao, S.-H. Cao, S.-L. Cai, X.-H. Cai and Y.-Q. Li, *Nanoscale*, 2017, **9**, 433–439.
25 B. Yameen, M. Ali, R. Neumann, W. Ensinger, W. Knoll and O. Azzaroni, *Small*, 2009, **5**, 1287–1291.
26 M. Zhang, X. Hou, J. Wang, Y. Tian, X. Fan, J. Zhai and L. Jiang, *Adv. Mater.*, 2012, **24**, 2424–2428.
27 R. Karnik, R. Fan, M. Yue, D. Li, P. Yang and A. Majumdar, *Nano Lett.*, 2005, **5**, 943–948.
28 M. Fuest, C. Boone, K. K. Rangharajan, A. T. Conlisk and S. Prakash, *Nano Lett.*, 2015, **15**, 2365–2371.
29 S. W. Nam, M. J. Rooks, K. B. Kim and S. M. Rossnagel, *Nano Lett.*, 2009, **9**, 2044–2048.
30 G. Laucirica, W. A. Marmisollé, M. E. Toimil-Molares, C. Trautmann and O. Azzaroni, *ACS Appl. Mater. Interfaces*, 2019, **11**, 30001–30009.
31 G. Pérez-Mitta, W. A. Marmisollé, C. Trautmann, M. E. Toimil-Molares and O. Azzaroni, *Adv. Mater.*, 2017, **29**, 1700972.
32 G. Pérez-Mitta, W. A. Marmisollé, C. Trautmann, M. E. Toimil-Molares and O. Azzaroni, *J. Am. Chem. Soc.*, 2015, **137**, 15382–15385.
33 E. B. Kalman, O. Sudre, I. Vlassiouk and Z. S. Siwy, *Anal. Bioanal. Chem.*, 2009, **394**, 413–419.
34 M. Nishizawa, V. P. Menon and C. R. Martin, *Science*, 1995, **268**, 700–702.
35 G. Laucirica, V. M. Cayón, Y. Toum Terrones, M. L. Cortez, M. E. Toimil-Molares, C. Trautmann, W. A. Marmisollé and O. Azzaroni, *Nanoscale*, 2020, **12**, 6002–6011.
36 Q. Zhang, Z. Zhang, H. Zhou, Z. Xie, L. Wen, Z. Liu, J. Zhai and X. Diao, *Nano Res.*, 2017, **10**, 3715–3725.
37 Q. Zhang, J. Kang, Z. Xie, X. Diao, Z. Liu and J. Zhai, *Adv. Mater.*, 2017, **30**, 1703323.
38 M. E. G. Lyons, *Electroactive Polymer Electrochemistry*, Springer, US, Boston, MA, 1st edn, 1994.
39 G. Pérez-Mitta, W. A. Marmisolle, L. Burr, M. E. Toimil-Molares, C. Trautmann and O. Azzaroni, *Small*, 2018, **14**, 1703144.
40 P. Yu. Apel, I. V. Blonskaya, O. L. Orelovitch and S. N. Dmitriev, *Nucl. Instrum. Methods Phys. Res., Sect. B*, 2009, **267**, 1023–1027.
41 M. E. Toimil-Molares, *Beilstein J. Nanotechnol.*, 2012, **3**, 860–883.
42 C. Trautmann, in *Ion Beams in Nanoscience and Technology*, ed. R. Hellborg, H. J. Whitlow and Y. Zhang, Springer-Verlag, Berlin, Heidelberg, 2009, pp. 369–387.
43 R. Tucceri, *Poly(o-aminophenol) Film Electrodes*, Springer International Publishing, Cham, 1st edn, 2013.

44 F. J. Rodríguez Nieto and R. I. Tucceri, *J. Electroanal. Chem.*, 1996, **416**, 1–24.
45 R. I. Tucceri, C. Barbero, J. J. Silber, L. Sereno and D. Posadas, *Electrochim. Acta*, 1997, **42**, 919–927.
46 C. Barbero, J. J. Silber and L. Sereno, *J. Electroanal. Chem.*, 1989, **263**, 333–352.
47 H. J. Salavagione, J. Arias, P. Garcés, E. Morallón, C. Barbero and J. L. Vázquez, *J. Electroanal. Chem.*, 2004, **565**, 375–383.
48 A. J. Bard and L. R. Faulkner, *Electrochemical Methods. Fundamentals and Applications*, Wiley, USA, 2nd edn., 2001.
49 K. Yamada, R. Gasparac and C. R. Martin, *J. Electrochem. Soc.*, 2004, **151**, E14.
50 C. Barbero, J. Zerbino, L. Sereno and D. Posadas, *Electrochim. Acta*, 1987, **32**, 693–697.
51 A.-H. A. Shah and R. Holze, *J. Electroanal. Chem.*, 2006, **597**, 95–102.
52 G. Socrates, *Infrared and Raman characteristic group frequencies: tables and charts*, John Wiley & Sons, Ltd, 3rd edn, 2001.
53 M. Tagliazucchi and I. Szleifer, *Chemically Modified Nanopores and Nanochannels*, Elsevier Inc., 1st edn, 2016.
54 G. Pérez-Mitta, A. G. Albesa, M. E. Toimil-Molares, C. Trautmann and O. Azzaroni, *ChemPhysChem*, 2016, **17**, 2718–2725.
55 M. Kasuya, T. Sogawa, T. Masuda, T. Kamijo, K. Uosaki and K. Kurihara, *J. Phys. Chem. C*, 2016, **120**, 15986–15992.
56 R. I. Tucceri and D. Posadas, *J. Electroanal. Chem. Interfacial Electrochem.*, 1985, **191**, 387–399.
57 Y. Lapitsky, *Curr. Opin. Colloid Interface Sci.*, 2014, **19**, 122–130.
58 A. L. P. Fernandes, W. A. Morais, A. I. B. Santos, A. M. L. de Araújo, D. E. S. dos Santos, D. S. dos Santos, F. J. Pavinatto, O. N. Oliveira, T. N. C. Dantas, M. R. Pereira and J. L. C. Fonseca, *Colloid Polym. Sci.*, 2005, **284**, 1–9.
59 G. Pérez-Mitta, W. A. Marmisollé, A. G. Albesa, M. E. Toimil-Molares, C. Trautmann and O. Azzaroni, *Small*, 2018, **14**, 1702131.
60 S. E. Herrera, M. L. Agazzi, M. L. Cortez, W. A. Marmisollé, C. Bilderling and O. Azzaroni, *Macromol. Chem. Phys.*, 2019, **220**, 1900094.
61 S. E. Herrera, M. L. Agazzi, M. L. Cortez, W. A. Marmisollé, M. Tagliazucchi and O. Azzaroni, *ChemPhysChem*, 2019, **20**, 1044–1053.
62 M. E. Carbone, R. Ciriello, S. Granafei, A. Guerrieri and A. M. Salvi, *Electrochim. Acta*, 2015, **176**, 926–940.
63 K. Lin, C.-Y. Lin, J. W. Polster, Y. Chen and Z. S. Siwy, *J. Am. Chem. Soc.*, 2020, **142**, 2925–2934.
64 R. I. Tucceri, *J. Electroanal. Chem.*, 2003, **543**, 61–71.
65 M. H. A. Haider, M. Ali and W. Ensinger, *Chem. Phys. Lett.*, 2021, **767**, 138349.
66 Y. He, D. Gillespie, D. Boda, I. Vlassiouk, R. Eisenberg and Z. Siwy, *J. Am. Chem. Soc.*, 2009, **131**, 5194–5202.
67 S. X. Li, W. Guan, B. Weiner and M. A. Reed, *Nano Lett.*, 2015, **15**, 5046–5051.
68 M. Fuest, K. K. Rangharajan, C. Boone, A. T. Conlisk and S. Prakash, *Anal. Chem.*, 2017, **89**, 1593–1601.